Check for updates

ADVANCED MATERIALS
www.advmat.de

3R Electronics: Scalable Fabrication of Resilient, Repairable, and Recyclable Soft-Matter Electronics

Mahmoud Tavakoli, Pedro Alhais Lopes, Abdollah Hajalilou, André F. Silva, Manuel Reis Carneiro, José Carvalheiro, João Marques Pereira, and Aníbal T. de Almeida*

E-waste is rapidly turning into another man-made disaster. It is proposed that a paradigm shift toward a more sustainable future can be made through soft-matter electronics that are resilient, repairable if damaged, and recyclable (3R), provided that they achieve the same level of maturity as industrial electronics. This includes high-resolution patterning, multilayer implementation, microchip integration, and automated fabrication. Herein, a novel architecture of materials and methods for microchip-integrated condensed soft-matter 3R electronics is demonstrated. The 3R function is enabled by a biphasic liquid metal-based composite, a block copolymer with nonpermanent physical crosslinks, and an electrochemical technique for material recycling. In addition, an autonomous laser-patterning method for scalable circuit patterning with an exceptional resolution of <30 µm in seconds is developed. The phase-shifting property of the BCPs is utilized for vapor-assisted "soldering" circuit repairing and recycling. The process is performed entirely at room temperature, thereby opening the door for a wide range of heat-sensitive and biodegradable polymers for the next generation of green electronics. The implementation and recycling of sophisticated skin-mounted patches with embedded sensors, electrodes, antennas, and microchips that build a digital fingerprint of the human electrophysiological signals is demonstrated by collecting mechanical, electrical, optical, and thermal data from the epidermis.

1. Introduction

Today, e-waste production has reached an alarming level of 7 kg person^{-1} year^{-1}.[1] Approximately 20% of the e-waste is sent for recycling, from which we recover only a small percentage of precious metals, particularly gold.[2] The rapid advances in smart packaging, printed electronics, sensing stickers, wearable health-monitoring patches, and smart e-textiles could result in the production of billions of disposable electronics in the next years. There are already commercial examples of disposable electronics patches for patient monitoring, continuous glucose tracking, sensorized diapers, and underwear for incontinence management, and electrochemical sensor kits for sweat, saliva, and blood analysis. As technological barriers to implementing disposable soft-matter electronics are being rapidly eliminated, large-scale use of disposable patches is foreseen in hospitals, elder care units, and professional athletes.

Despite the social and economic advantages of these systems, this race for a "smarter" future comes at the cost of exponentially increasing e-waste production. The disposal of billions of systems that contain highly processed microchips and scarce metals will lead us to another man-made disaster. Complex biomonitoring systems contain many analog and digital components that can be reutilized. Therefore, the possibility of recycling these components, as well as the metals from printed circuits, should be considered. As we are shifting toward short-term use of electronics, we need to urgently rethink the material architecture to allow recyclability before any fabrication procedure becomes dominant. The traditional 3Rs politics (reuse, reduce, and recycle) is not pertinent in the emerging wearable monitoring applications. Reutilization is not permitted due to hygiene reasons, and the trend of use is only at the beginning of an exponential growth.

In the last few years, this problem has attracted the attention of scientists. Recently, there was a report on a disposable and biodegradable supercapacitor,[3] and there have been a few studies on the recovery of Ag from used batteries through electrowinning.[4–8] In the field of transient electronics, some works focused on biodegradable circuits over starch[9]

M. Tavakoli, P. Alhais Lopes, A. Hajalilou, A. F. Silva, J. Carvalheiro, J. Marques Pereira, A. T. de Almeida
Soft and Printed Microelectronics Lab
Institute of Systems and Robotics
University of Coimbra
Coimbra 3030-290, Portugal
E-mail: mahmoud@isr.uc.pt

M. Reis Carneiro
Soft Machines Lab
Mechanical Engineering
Carnegie Melon University
Pittsburgh, PA 15213, USA

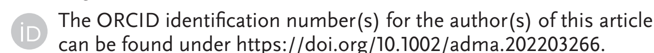
The ORCID identification number(s) for the author(s) of this article can be found under https://doi.org/10.1002/adma.202203266.

© 2022 The Authors. Advanced Materials published by Wiley-VCH GmbH. This is an open access article under the terms of the Creative Commons Attribution-NonCommercial-NoDerivs License, which permits use and distribution in any medium, provided the original work is properly cited, the use is non-commercial and no modifications or adaptations are made.

DOI: 10.1002/adma.202203266

and poly(lactic-*co*-glycolic acid) (PLGA).[10] Further, soluble poly(vinyl alcohol) (PVA) and polyimine with dynamic covalent bonds were used as the packaging materials, which allowed the recovery of liquid metal (LM) from the circuit.[11,12] A review of biodegradable transient electronics can be found in.[13] While promising for some applications, transient and biodegradable electronics are generally composed of nonresilient materials that function for a short time and in specific environments. For instance, PVA falls short in applications that demand resilience to humidity. In general, the degradation profiles of the designed materials should accommodate the required device lifetimes.[14]

In two recent studies, LM-embedded elastomers with crosslinked polyurethane (PU)[15] and SIS[16] were used for fabricating stretchable interconnects, from which LM could be recovered. However, these composites require a mechanical sintering step to form conductive traces, which hinders the autonomous fabrication of high-resolution printed circuits. In addition, a Ga–In–SiO_2 paste was introduced,[17] from which LM could be recovered.

These advances are promising for the move toward recyclable electronics. However, the previously presented methods lack the required maturity, including the desired patterning resolution and the automation level necessary for industrial applications. Therefore, they fall short compared to the current high throughput printed circuit board (PCB) manufacturing, in terms of high-resolution patterning, multilayer implementation, and scalable and automated fabrication. The reasons for this include the shortcomings of the existing LM composites, e.g., the need for mechanical sintering, the smearing behavior, lack of mechanical integrity, and lack of adhesion to the substrate that hinders efficient printing of the circuit. Recently, we addressed some of these problems by demonstrating liquid metal-based biphasic composites that are sinter-free and nonsmearing.[18–20] However, the resolution of the circuit printing was limited because of the mechanical limitations of the extrusion-based printing. Therefore, it was impossible to develop circuits with the same resolution as current rigid PCBs that use state-of-the-art integrated circuits such as surface-mount device (SMD) microchips. Real progress toward 3R electronics only happens if we can demonstrate novel fabrication techniques that in one hand rely on resilient, repairable, and recyclable materials, and on the other hand can compete with existing techniques in terms of patterning resolution, multilayer implementation, microchip integration, and autonomous fabrication.

Here, we present a novel architecture for scalable, autonomous, and high-resolution fabrication of 3R electronics through direct laser patterning of “3R materials,” including biphasic printable liquid metal composites and “reversible” tough block copolymers (BCPs), which benefit from a high elasticity and nonpermanent physical crosslinking. The resulting conductive traces are ultraresilient to mechanical strain and can withstand >1700% of strain before an electrical break. We demonstrate the integration of miniature silicon chips for data acquisition, processing, and wireless communication through room-temperature chemical soldering by taking advantage of reversible polymer bonds in block copolymers. We take advantage of the same reversible bonds for repairing the damaged circuits and exploit these nonpermanent physical crosslinks for the rapid and efficient recovery of silicon chips and other materials, including textile, polymer films, eutectic gallium indium (EGaIn) liquid metal, silver, and ferrite. We show how these materials can be employed for fabricating complex electronic devices. We then compare two different biphasic composites based on Ag and Fe and demonstrate techniques for recycling the metal elements from the biphasic amalgams for both cases. This includes using magnetic force to separate metals in EGaIn–Fe–SIS composite and a combination of chemical and electrochemical processes, such as leaching and electrowinning, for recovering individual metals from EGaIn–Ag–SIS composite. We compare these two composites in terms of smearing behavior, microstructure integrity, and ease of recycling.

We also demonstrate a high-resolution laser patterning technique that significantly improves the circuit patterning speed by 3–8× (depending on circuit size) and the resolution by ≈10×, compared to our previous work on digital printing.[19] Usually, a circuit resolution better than 200 µm is desired for modern silicon chips. The low-cost laser processing technique presented herein allows patterning traces with 30 µm width, compared to 300 µm in digital printing. Adding to this the single-step vapor-assisted microchip integration, this work paves an important path toward scalable fabrication of 3R electronics.

We demonstrate various examples of condensed soft-matter circuits that embed the necessary state-of-the-art SMD microchips and show examples of skin-mounted patches and e-textiles that monitor mechanical, electrical, optical, and thermal changes in the epidermis. In one example, we show a large and complex multisensor e-skin with several laser-patterned strain gauges that integrates all the required microchips for acquisition, amplification, processing, and wireless communication. This patch continuously obtains a digital fingerprint of the skin strain profile at multiple positions and direction and utilizes this for classification of human activities, including breathing, eating, and various sports activities on the neck and torso. All these circuits comply with the 3Rs electronics concept. They are resilient to mechanical strain, repairable if damaged, and recyclable after disposal. We successfully recovered and reintegrated these microchips 10 times.

The entire fabrication process, including the deposition, patterning, and microchip “soldering,” is performed at room temperature. Elimination of temperature from the sintering process (as common in printed electronics) and from the soldering process is an important step toward green electronics as it enables the fabrication of electronics over a wide range of heat-sensitive substrates that were not previously possible. At the same time, this reduces energy consumption. A recent review of emerging biodegradable elastomers and gels for elastic electronics can be found in ref. [21].

In summary, to achieve the objectives of 3R electronics, we tackled three main challenges. First, we introduced a novel architecture for soft-matter materials such as conductive composites and substrates that satisfy the 3R objectives, do not require thermal sintering, and embed “reversible” functions that can be exploited for healing, soldering, and recycling. Second, we developed autonomous fabrication techniques, including high-resolution digital patterning and single-step microchip “soldering,” and third, we developed supporting technologies for recycling the materials and components. These

© 2022 The Authors. Advanced Materials published by Wiley-VCH GmbH

challenges are interrelated and must be addressed simultaneously to guarantee a real step toward sustainable 3R electronics. By addressing these challenges, this work lays the foundation for the next generation of recyclable soft-matter electronics that can compete with current PCB manufacturing techniques, thus paving an important step toward green fabrication and sustainable and responsible application.

2. Results

Figure 1 shows the concept and building blocks of 3R electronics. 3R electronics relies on a series of 3R materials (Figure 1A) that can be processed to fabricate complex circuits through autonomous and room-temperature fabrication techniques (Figure 1B and Video S1, Supporting Information) and applied to a wide range of applications like wearable monitoring (Figure 1C). After disposal, these devices can be recycled to obtain the costly elements and microchips (Figure 1D). This is especially important as many of these patches are intended to be used only for a few hours. We should rely on a material architecture compatible with the 3R objectives to enable these objectives. Referring to Figure 1A, as a 3R conductor, we use a biphasic LM composite composed of a block copolymer, EGaIn LM, and conductive microfillers. This ternary composite is conductive, stretchable, and sinter-free. The use of EGaIn LM enables a combination of high conductivity, self-healing property, and high resilience, which is inherent in its liquid phase. The main objective of the microfiller is to percolate between the LM droplets, which grants the composite conductivity right after deposition. Previous efforts at making a liquid metal embedded elastomer resulted in printable composites but required a mechanical sintering step to gain conductivity.[22] Choosing from a wide range of available conductive fillers allows fine-tuning the viscosity, printability, and electromechanical properties of the composite. The choice of filler has a direct and substantial influence on the properties of the ink, including its recyclability, smearing behavior, homogeneity, and ability to retain the liquid metal when subject to mechanical strain and pressure. We recently demonstrated a version of this ink that uses Ag flakes as microparticles.[19,20] This

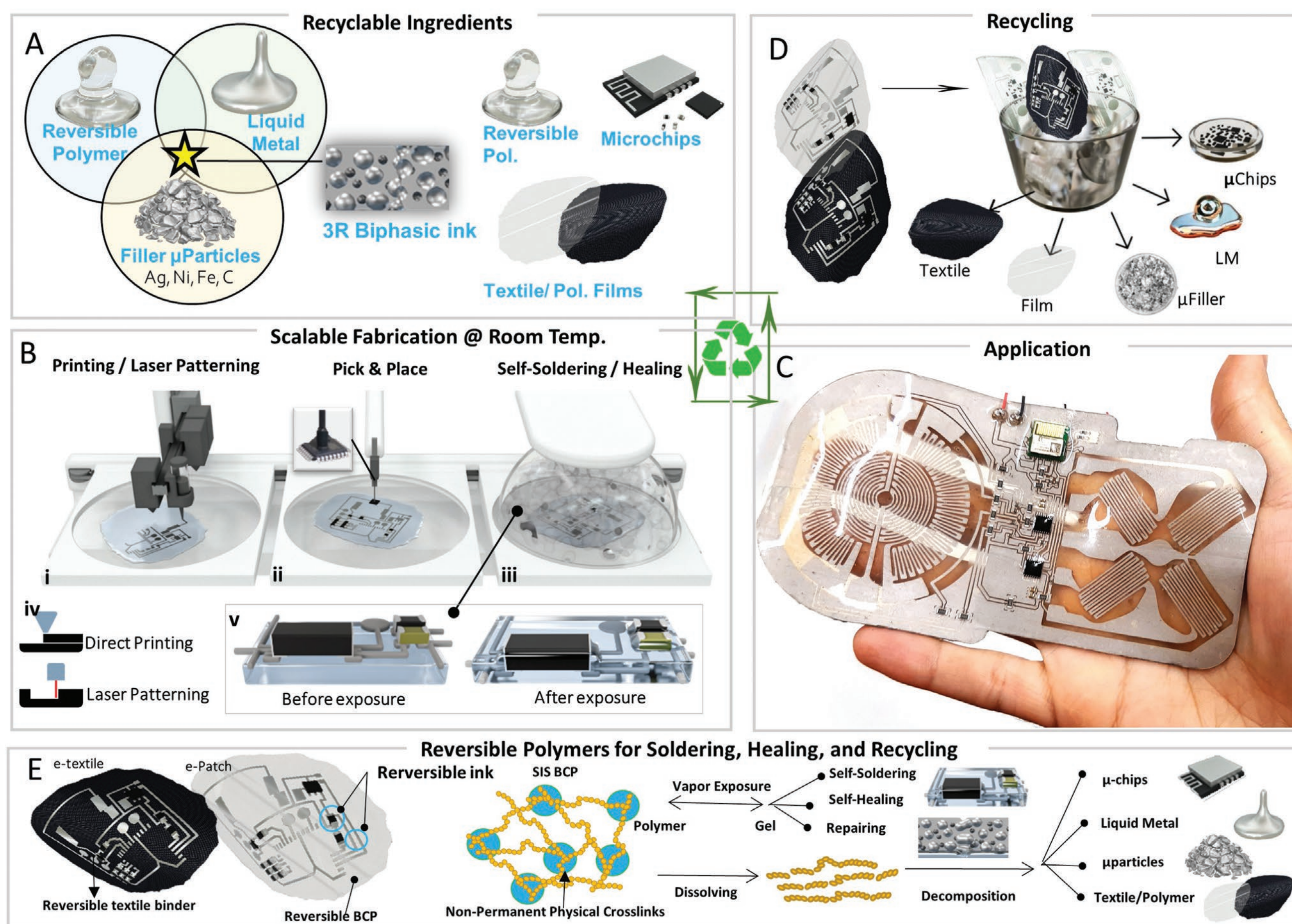

Figure 1. 3R Electronics. A) Constitutional materials, including biphasic liquid metal-based inks and reversible polymers. B) Autonomous fabrication techniques including printing/laser patterning i), Pick and place ii), and vapor-assisted soldering and healing iii). Thanks to the reversible polymers, the microchips penetrate the ink and the substrate, resulting in a seamless integration into the circuit v). C) Example of a laser patterned soft-matter circuit with eight strain gauges and state of the art SMD microchips for processing, amplification, and communication. D) The concept for recovery of the elements from 3Rs electronics, based on dissolving reversible polymeric matrix. E) Utilization of reversible polymers with nonpermanent physical crosslinks, as the substrate, e-textile adhesive, and binder in ink, contributes to self-soldering, Self-healing, repairing and recycling.

© 2022 The Authors. Advanced Materials published by Wiley-VCH GmbH

can be extended to other conductive particles to obtain different electromechanical properties. This includes ferromagnetic particles, further discussed in this work.

We use SIS (styrene–isoprene–rubber) BCP as the elastomeric binder in the composite and as well for the substrate. SIS is a thermoplastic elastomer and a triblock copolymer, including both permanent chemical crosslinks and physical crosslinks. Longer chains of chemically crosslinked isoprene sequences include polystyrene blocks at the end of their chains (Figure 1E). These polystyrene blocks collect in small domains through physical crosslinks. Therefore, SIS BCP benefits from a reversible phase-shifting property and rapid solubility, which are exploited in this work for several processes. Unlike many polymers that only soften in contact with solvents, SIS can be either softened or fully dissolved in the solvent, depending on the exposure time and intensity.

This property is exploited in this work for (Figure 1E): healing of the microcracks that are formed on the ink/substrate after deposition due to solvent evaporation; repairing of circuits that suffered severe damage or a thorough cut; "soldering" of SMD components through solvent vapor exposure that causes a reversible transition from polymer to gel state in the SIS BCP; and recycling the circuit microchips, metals, and polymer/textile substrate by decomposition of the circuit to its constitutional elements through dissolving the circuit in the solvent (C6H5CH3). The use of polymers with nonpermanent bonds (e.g., physical crosslinks) is the key to achieving the objectives of 3R. Moreover, SIS BCP provides excellent adhesive properties, resilience, elasticity, and toughness.

Referring to Figure 1B, automated room temperature fabrication of hybrid stretchable circuits starts with the deposition and patterning of ink through either direct ink writing (DIW) or laser patterning (Figures 1B-i,iv, and Video S1, Supporting Information). After patterning the circuit, the microchip components are placed over it using a pick and place machine (Figure 1B-ii), and then it is exposed to toluene vapor (Figure 1B-iii). Vapor is generated using a home-made system composed of a spray nozzle that creates microdroplets of the solvent at room temperature through intensified sonic energy using compressed air as the energy source. The resulting atomized droplets of toluene cause a phase transition in the polymer, from solid to semisolid gel, which happens in both the SIS substrate and the SIS-containing conductive ink (Figure 1B-v). In this state, microchips penetrate the softened ink and the substrate (Figure 1B-v). Once the vapor stimuli are removed, microchips are mechanically locked into the substrate from 5 facets, also assisted by the excellent adhesion properties of the SIS BCP. Compared to the existing techniques, the soldering process is convenient, as it does not require selective deposition of solder paste or conductive adhesives. In fact, the printed ink and substrate act as the soldering matter, thus eliminating the need for deposition and sintering of the solder paste. The entire process is performed at the room temperature, including the creation of the solvent vapor and the "soldering" process. The room temperature process is important for the move toward recyclable electronics. Today, the choice of the substrate for the fabrication of rigid and flexible PCBs is limited to a few heat-resistive substrates. For instance, most of today's flexible circuits are created over polyimide, which is not stretchable, soluble, or recyclable. The elimination of the temperature from the entire fabrication process opens the door to a wider range of previously impossible substrates due to their limited heat resistance, including those with reversible functions. Moreover, a room-temperature process reduces energy consumption.

Figure 1C demonstrates an example of a 3R circuit created with this technique that embeds 8 laser-patterned strain gauges, miniaturized SMD electronic components for signal acquisition, amplification, and processing, and bluetooth low energy (BLE) for communication. Referring to Figure 1D, both patch and e-textile circuits can be decomposed to their "ingredients" thanks to the existing nonpermanent physical crosslinks in the BCPs (Figure 1E).

2.1. Ink Synthesis and Circuit Patterning

As seen in **Figure 2**A, the EGaIn–Ag–SIS composite is prepared by dissolving SIS block copolymers (Sigma-Aldrich) in a toluene solution, followed by mixing ≈5 µm Ag flakes (Silflake Technic Inc.) and then EGaIn.

The alternative EGaIn–Fe–SIS composite is prepared similarly but replaces the Ag flakes with ferromagnetic particles (Fe_3O_4 magnetite 52 µ, 99%, CAS: 1309-38-2). Circuits can be patterned through direct ink writing (Figure 2B,C) or laser patterning (Figure 2D–F).

Direct ink writing brings several advantages, including single-step fabrication, the possibility of creating thick and highly conductive traces, and eliminating the need for a stencil. We have successfully printed the ink over textile and various polymers, including medical-grade wound dressing adhesive (Tegaderm-Figure 2B-ii). Figure 2C demonstrates an example of a pressure mapping e-textile that is fabricated through printing a double-layer mesh of parallel plate capacitive sensors. Figure 2D shows an example of a printed circuit applied over polymer film and transferred to a glove for mapping the pressure applied to the fingertips and bending of the joints. An example of surface texture classification is also presented.

One disadvantage of this printing technique is that the circuit resolution is limited by the size of the nozzle (≈300 µm linewidth and spacing). While this is sufficient for many applications, increasingly miniaturized SMD microchips require a resolution as low as 100 µm. To overcome this limitation, we developed a laser patterning technique that significantly improves the resolution by ≈10×. We demonstrate high-resolution circuits with a line width and spacing of 25 µm and 52 µm, respectively. Figure S1 (Supporting Information) shows images of the patterned traces and optical profilometry analysis. Laser patterning is performed using a master oscillator power amplifier (MOPA) fiber laser with a 1064 nm infrared wavelength. This laser is very accessible and is widely used by local shops for engraving metals. First, a PVA sacrificial layer is applied over the glass, followed by applying a film of the conductive ink using a thin-film applicator, which is then patterned using the MOPA laser. Next, a layer of SIS BCP is applied over the circuit, and the PVA layer is dissolved in water to peel the circuit. In this way, multiple circuits can be patterned in a few minutes (Figure 2E).

Both printing and laser patterning techniques are shown in Video S1 (Supporting Information). Optical profilometer

© 2022 The Authors. Advanced Materials published by Wiley-VCH GmbH

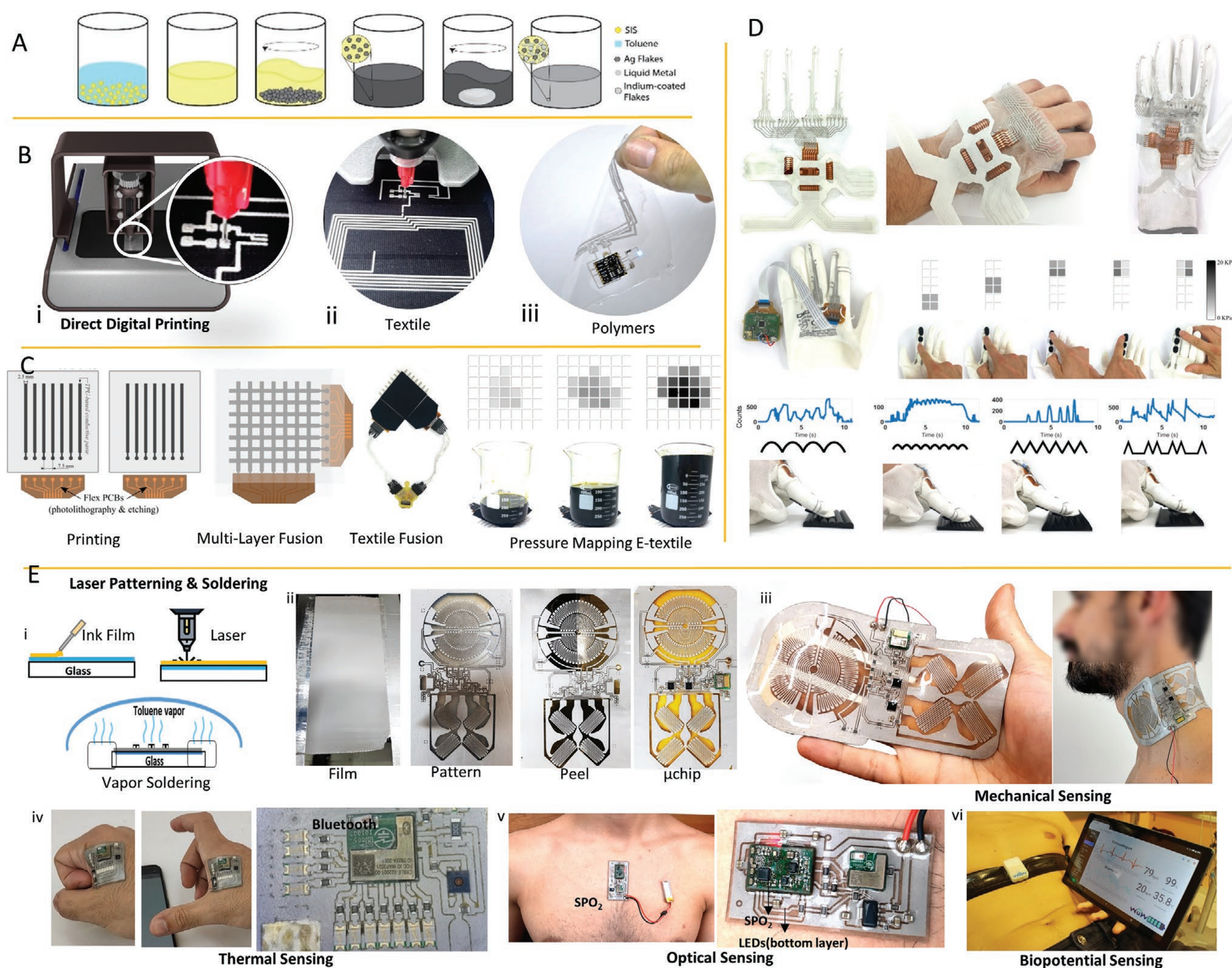

Figure 2. A) Synthesis of sinter-free stretchable biphasic ink. B) Digital Printing of e-patch and e-textile circuits C) Example of a pressure mapping e-textile fabricated through digital printing. D) Example of a wearable glove with printed bending and pressure sensors, its application in pressure sensing, and surface texture classification. E) High-resolution Laser Patterning of the circuits using an accessible IR laser and Single-step vapor-assisted soldering of miniaturized components: i) Example of the fabrication steps. ii) No solder material or thermal treatment is necessary. Examples of chip-integrated soft-matter epidermal biostickers for mechano-sensing iii), thermal iv), optical v), and electrical sensing vi). These patches can be used for monitoring respiration and physical activities iii), body temperature iv), heart rate, and SPO2 v). The belt presented in E-iv measures ECG, heart rate, respiration, temperature, and body motions simultaneously.

images of Figure S1 (Supporting Information) show that the single-layer film thickness is ≈15 µm. The average conductivity for 5 lines of 100 µm width for a single layer coat was 2.1×10^5 S m^{-1}. Figure S2 (Supporting Information) shows the detailed steps of the laser patterning process. Compared to digital printing, laser patterning provides better resolution and faster fabrication. For instance, the circuit shown in Figure 2F-iii takes ≈320 s via digital printing versus 44s in laser patterning. In addition, our attempts to fabricate this circuit via digital printing failed due to the complexity and the resolution.

In the case of hybrid circuits with integrated microchips, these components are integrated into the circuit using the toluene vapor exposure technique. As demonstrated in Figure S3 (Supporting Information), the laser processing and vapor-assisted soldering techniques allow the simultaneous fabrication of multiple circuits. Figure 2E-ii and Figure S4 (Supporting Information) show a step-by-step example of fabricating a soft-matter circuit. Figure 2E-iii and Video S4 (Supporting Information) show the resulting circuit: a wireless Mechanosensing patch that integrates eight laser patterned strain gauges and several miniaturized SMD components, including BLE for wireless communication, a processor, amplifiers, resistors, and several light emitting diodes (LEDs) for displaying information. Figure 2E-iv and Figure S3 (Supporting Information) show a wireless temperature monitoring patch. Figure 2E-v, Figure S5 (Supporting Information), and Videos S2 and S3 (Supporting Information) demonstrate a complex circuit for pulse oximetry and monitoring blood oxygen levels. Here, components are installed on both sides of the patch, allowing LEDs and photodetectors to interface with the epidermis. Figure 2E-iii–vi shows four examples of skin-interfacing soft-matter patches for mechanical, thermal, optical, and electrical (biopotentials) sensing. Overall,

© 2022 The Authors. Advanced Materials published by Wiley-VCH GmbH

the materials and fabrication techniques presented here pave an important step toward scalable fabrication of high-resolution, chip-integrated soft-matter 3R electronics.

In order to create multilayer circuits, we used two different methods. The first technique consist of mounting the components on one side of the circuit through vapor-assisted soldering, peeling the circuit after addition of the encapsulating SIS layer, and mounting the component on the second layer of the ink through vapor-assisted soldering. Please see Section S4 of the Supporting Information, and also Figure S21 (Supporting Information) for additional details. This technique is simple, and fast, and permits epidermal electronics with sensors mounted on skin side, while processing and communication components mounted on the opposite side of the circuit. This allows reducing the overall footprint of the sensor. This is the case for the circuit shown in Figure 2E-v, with LEDs and photo detectors on the skin-interfacing layer, and Bluetooth and processing chips on the opposite side. The disadvantage of this technique is that it cannot be extended for additional layers.

The second method permits fabrication of multilayer circuits through the stacking technique. First single-layer PCBs are produced via laser patterning, with the connection points exposed. These layers are then joined together through vapor-assisted circuit fusion. See details of this process in Figure S22 (Supporting Information), and Section S4 of the Supporting Information. Figure S23 (Supporting Information) shows an example of a double layer coil antenna, with integrated LED. This coil antenna is used for harvesting energy from mobile phone's near field communication (NFC) coil, and lighting the LED without the need for any battery. Inclusion of a second layer of the coil improves the energy harvesting efficiency, compared to a single-layer coil. Video S11 (Supporting Information) shows the functionality of this double layer circuit.

2.2. Electromechanical Characterization, and Repairing of the damaged circuits

Printed conductive traces produced by the referred materials and methods are very resilient and can withstand a record-breaking maximum strain tolerance of 1700% (**Figure 3**A-i). A microchip-integrated circuit can withstand strains of >500%

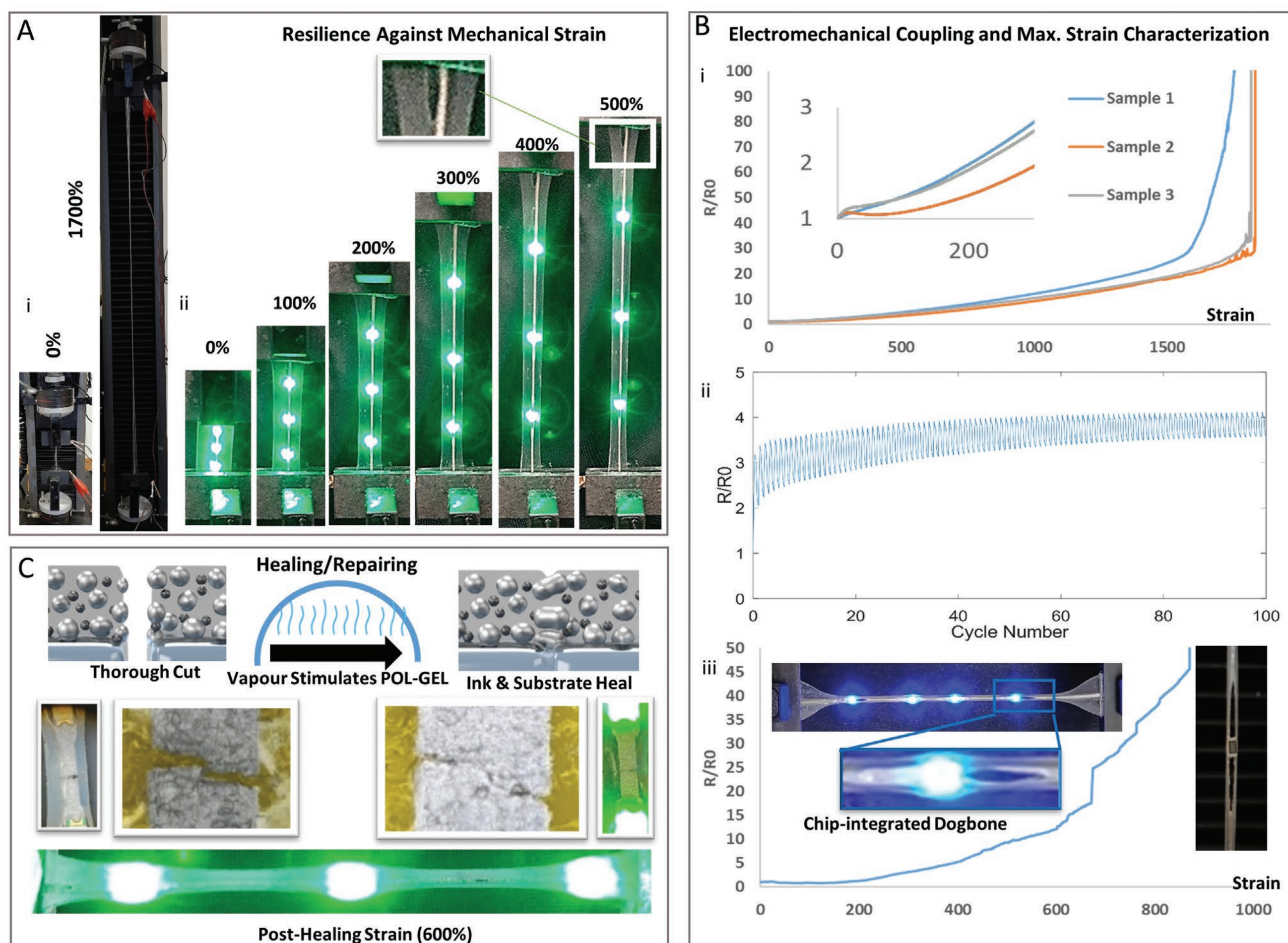

Figure 3. A) Printed trace without chip i) and with microchips ii) under strain. B) Electromechanical coupling of the circuits. Electrical resistance versus strain (i), repetitive cycle test for 30% strain ii), resistance v/s strain for microchip integrated circuit iii). Cracks are formed usually at >500% strain on the substrate and grow until mechanical failure. C) Vapor-assisted repairing of the circuit which was cut using a sharp knife, and the same circuit under 600% strain after healing.

© 2022 The Authors. Advanced Materials published by Wiley-VCH GmbH

(Figure 3A-ii,C-iii), a value >6× compared to previous studies that demonstrated microchip integrated circuits.[23–25] As seen in the insets of Figure 3A-ii, the mechanical failure does not necessarily happen on the chip interface. A premature mechanical failure sometimes occurs at the grippers of the characterization device. Figure 3B-I shows the electromechanical coupling of 3 printed circuits (no microchip) when subject to over 1500% mechanical strain. In addition to the extreme resilience, the circuits present a very modest gauge factor and a quasi-linear behavior until ≈1000% strain. Figure 3B-ii shows printed traces under 100 repetitive cycles with 30% applied strain. In the first 40 cycles, the R_0 value (resistance at 0% strain) increases slightly. However, this increase is only from initial value of ≈2 Ω to a final value of ≈3 Ω and then stabilizes. Figure 3B-iii shows resistance versus strain of a microchip integrated strain and an image of the sample under ≈900% strain, right before and right after the electrical failure. As expected, the failure happens at the rigid-soft interface at the edge of the microchip. The crack initiates at ≈700% strain, which is visible as an increase in the electrical resistance in Figure 3B-III. It is noteworthy that although this crack forms and grows under strain, the ink still maintains its connection to the LED from two edges of the crack.

Unlike the existing techniques wherein the SMD microchips are soldered or bonded to the conductive trace only from the bottom side, in this technique, microchips are surrounded on all 5 facets and adhere strongly to the substrate and ink due to the excellent adhesive properties of the SIS. Therefore, the stress concentration zone, i.e., the interface between the chip and the substrate, has increased substantially. Thus, this results in a significant (>6×) improvement over the state-of-the-art in the maximum strain tolerance of the chip-integrated circuits.[26,27] Note that the maximum strain tolerance for chip-integrated circuits largely varies depending on the size, number, and distribution of these microchips. In most previous works, characterization is performed with only a single chip.

In addition, 3R circuits are repairable in case of damage. Referring to Figure 3B, after making a thorough cut using a sharp blade, the circuit was repaired by the same solvent vapor exposure technique used for microchip interfacing. The repair is so efficient that the circuit could be subject to large strains. Figure 3C shows an example of a cut circuit that remains functional after the vapor exposure, even when subject to >600% strain. Exposing the circuit to the solvent vapor results in the expansion of the polymer volume and the weakening of the physical crosslinks between the polymer chains. This allows reconnection and rearrangement of the polymer chains, thus self-repairing the cut zone.

2.3. Recycling

Referring to **Figure 4**, both e-textile and hybrid patches can be recycled to their constitutional elements in a few simple steps. Figure 4A and Video S5 (Supporting Information) show the process for recovering the components from a hybrid microchip integrated patch. The circuit is first placed over a filter (mesh count 100T), then over a paper soaked with toluene, and then placed in a closed chamber. This generates an intense toluene vapor environment that dissolves the SIS substrate absorbed by the underlying paper. In this way, the ink and the components are separated from the substrate. The vapor-assisted substrate removal is a simple technique that allows facile recovery of the microchip components that are usually the costliest elements in the patch. Afterward, the concentrated ink, which is a metal-rich chunk with some remaining SIS polymer can be

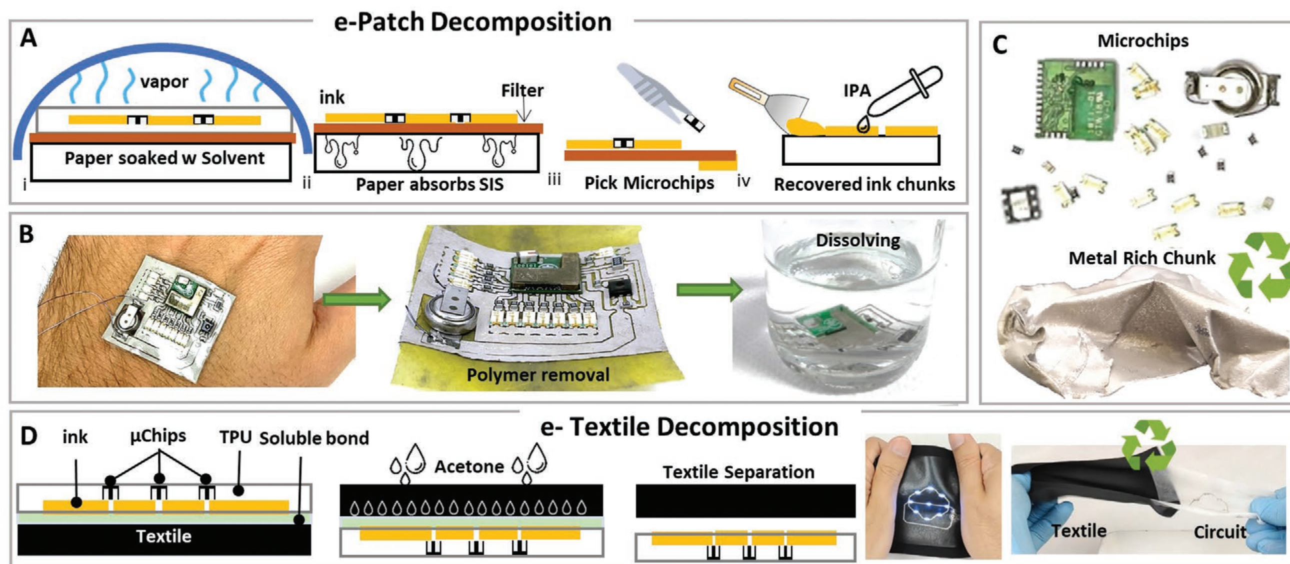

Figure 4. Recycling the e-patch and e-textile circuits. A) e.patch are first decomposed by a vapor-assisted substrate removal, allowing separation of the microchips and ink as a metal chunk. B) Example of wireless thermal monitoring patch on the skin, after polymer removal. An alternative method for removing components and the ink is direct dissolving. C) Microchips, battery, and metal chunk removed from the thermal patch. D) e-textile recycling starts with removing the acetone soluble bond between the e-patch and the textile. After the recovery of the textile, the e-patch is recycled using the same technique as (A).

© 2022 The Authors. Advanced Materials published by Wiley-VCH GmbH

collected. Alternatively, after removing the substrate, the filter that contains the ink and microchips can be placed in toluene for simultaneous recovery of all components. This latter technique is depicted in Figure 4B, which shows the decomposition of the laser patterned wireless temperature monitoring patch in Figure 2E. Figure 4c depicts the recovered microchips and the metal-rich chunk.

Figure 4D and Video S6 (Supporting Information) demonstrate the decomposition steps for the e-textile. A 3R e-textile is composed of a patch fused into the textile through heat transfer or solvent-vapor-assisted fusion. The process relies on a reversible and/or soluble thermoplastic such as SIS or thermoplastic poly urethane (TPU) that fuses seamlessly into textile fibers during the transfer process. As demonstrated in Figure 4C, to decompose the e-textile, it is first soaked with the solvent of the adhesive polymer. This dissolves the adhesive layer coated to the polymer, which permits peeling off the patch from the textile. Then, the patch can be recycled through the techniques shown in Figure 4A,B.

The recovered metal-rich chunk shown in Figure 4C contains EGaIn, metallic microfiller (Ag or Fe), and the remaining SIS polymer that could not be fully removed during the steps shown in Figure 4A. Therefore, the metal-rich chunk produced in this step requires further processing to recover the individual metals (**Figure 5**). In the case of EGaIn–Fe–SIS ink, the recovery of liquid metal and the ferromagnetic ferrite filler is straightforward through magnetic force (Figure 5A and Video S7, Supporting Information). We first mix the metal-rich chunk with an ecofriendly acid (citric acid). Citric acid removes the Ga_2O_3 oxide shell around the EGaIn droplets and therefore contributes to the separation of the EGaIn from the metal chunk. After removing the EGaIn, we remove the remaining SIS polymer by mixing the remaining chunk with Toluene. Finally, we collect the ferrite microparticles using a permanent magnet. As shown in Video S7 (Supporting Information), the particles maintain their original ferromagnetic property.

In the case of EGaIn–Ag–SIS (Figure 5B), we developed a mechano-chemical process based on gallium oxide dissolution in a basic solution, i.e., NaOH, accompanied by mechanical forcing exerted during mixing and sonication (see Videos S8 and the Experimental Section for details). After recovery of the LM, we obtain an Ag-rich chunk.

To recover the Ag from this chunk, we performed a leaching process that included further sonication to disperse particles and dissolve them in the sulfuric acid (See the Experimental Section for details). This allowed dissolving of Ag and the remaining EGaIn coating.

After the leaching, the Ag ions in the solution are transformed back into pure Ag without EGaIn contaminants using an electrowinning process. Then, the solution was poured into an electrochemical cell container, and glassy carbon electrodes were used as the cathode and anode. Pure Ag was recovered by applying a constant potential of 10 V for 4 h. At the cathode surface, Ag metal aggregates and forms a metal chunk, which falls to the bottom of the container after gaining some weight. Video S9 (Supporting Information) shows the process of collection of the Ag through electrowinning after the leaching step. The LM recovered from this process can be used directly for making a new ink. However, the Ag should be first transformed to flake form, in order to be usable for synthesis of the EGaIn–Ag–SIS ink.

It is interesting as well to discuss the role of gallium in the success of the leaching and electrowinning process. In one experiment we tested the leaching process in equal conditions for Ag-SIS composite, and an Ag-SIS composite with addition of EGaIn. The amount of EGaIn/Ag ratio was 0.65/1.65, which is considerably lower than the biphasic EGaIn–Ag–SIS composite. This composite was made in order to simulate the Ag-rich chunk that remains after recovery of EGaIn, and before the leaching process. Details of the experiment can be seen in Figure S18 (Supporting Information), and Section S3B of the Supporting Information. As a result, we found that existence of the EGaIn in the formulation helps in the leaching process. This can be as well seen in Videos S10 (Supporting Information), which compares the leaching process for both composites. As can be seen, from the composite that contains EGaIn, only SIS polymer is remained after 45 min of leaching, whereas no change in the composite without EGaIn is observed after 3 h of mixing. To the best of the authors' knowledge, this is the first time that combining sulfuric acid leaching and electrowinning for the extraction valuable silver from the biphasic conductive composite with high efficiency at room temperature has been discussed.

Figures S19 and S20 (Supporting Information), show the elemental analysis of the Ag obtained through electrowinning, showing that it is a pure Ag, with some remaining of sulfur from the sulfuric acid used in the leaching process.

In summary, the unique combination of materials, i.e., reversible block copolymers, EGaIn, and Ag in the composite, enabled the high efficiency of the recycling process.

Although the EGaIn–Fe–SIS has fewer steps to recover the ink elements, there exists a trade-off between the ease of recovery and the ink properties. Figure 5C,D demonstrate optical images of a nonencapsulated EGaIn–Fe–SIS and an EGaIn–Ag–SIS, respectively, after subjecting them to 10 cycles of 100% strain. As can be seen, the EGaIn–Ag–SIS remain nonsmearing while some LM droplets are separated from the EGaIn–Fe–SIS composite. Therefore, the choice between the composites is a trade-off. Circuits based on EGaIn–Fe–SIS are easier to recycle but more complex to fabricate, as they need an encapsulation layer to remain nonsmearing when subject to mechanical strain. Scanning electron microscopy (SEM) from the top surface (Figure 5E), and cross-section (Figure 5F) of the EGaIn–Fe–SIS composite, and EGaIn–Ag–SIS (Figure 5G,H), shows that the latter is considerably more homogenous. The liquid phase EGaIn in EGaIn–Ag–SIS is more entangled with the solid phase Ag, thus resulting in the liquid metal being retained in the microstructure when subject to the mechanical strain. However, this comes at the cost of a more complex element recovery process. Figures S9, S10, S11, and S12 (Supporting Information), and the related discussion in the supporting information provide additional insights about the microstructure of the EGaIn–Ag–SIS and EGaIn–Fe–SIS biphasic composites. Through SEM and energy dispersive X-ray spectroscopy (EDS) from the top and cross-section of the printed samples, we demonstrate the microstructure and material distribution for both composites, and show formation of $AgIn_2$ intermetallic component (IMC). This IMC permits

© 2022 The Authors. Advanced Materials published by Wiley-VCH GmbH

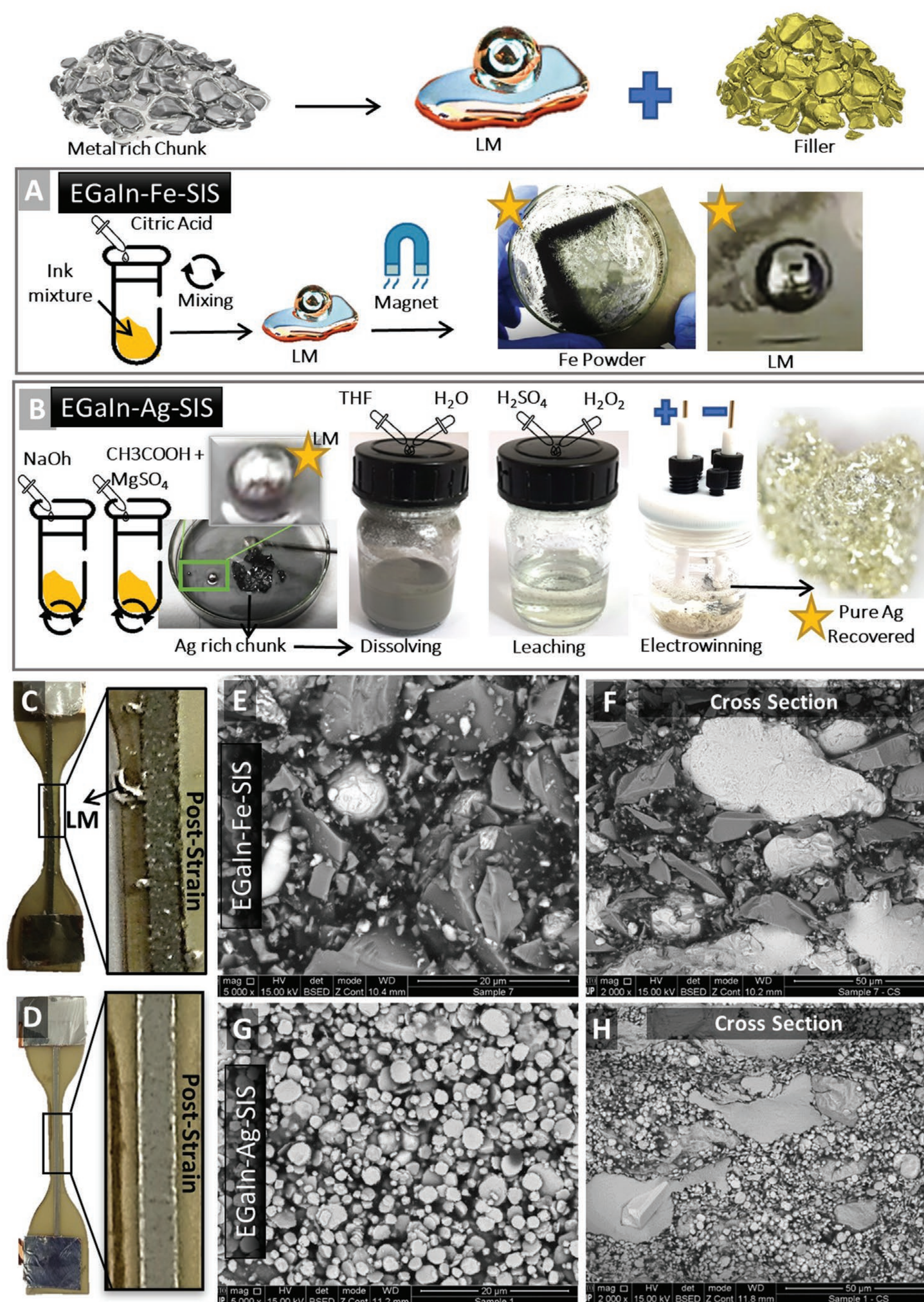

Figure 5. Extraction of the metal elements from the recovered metal chunk in the previous step. A) Method for separation of LM and Ferrite from EGaIn–Fe metal chunk, using magnetic force. B) Method for separation of Ag, and EGaIn, based on the mechano-chemical procedure followed by dissolving, leaching and Electrowinning. C) Fe–EGaIn–SIS composite after 100% mechanical strain. The phase separation is expectable due to the nonhomogeneous microstructure as shown in SEM analysis: E) top surface and F) cross-section. D) Optical image of an Ag–EGaIn–SIS sample post-strain. SEM microscopy from G) top surface and H) Cross-section

formation of a more homogenous composite that does not suffer from phase separation, and thus results in the desired nonsmearing behavior, albeit at the cost of making recycling more difficult.

In addition, it can be seen from Figure S12 (Supporting Information), that a line printed through extrusion printing results in a line thickness of ≈100 µm, which is 5.5 times higher than the 15 µm thickness in the circuits produced by thin/film coating and laser patterning (referring to optical profilometer images in Figure S1 in the Supporting Information). The thickness of the printed trace, had an inverse linear relation with its electrical resistance, according to the Pouillet's law of electricity. While this reduced resistance is generally appreciated in digital circuits, it also increases the ink consumption. Besides the laser patterned circuits were able to deliver the intended function in all laser patterned digital circuits shown in Figure 2.

© 2022 The Authors. Advanced Materials published by Wiley-VCH GmbH

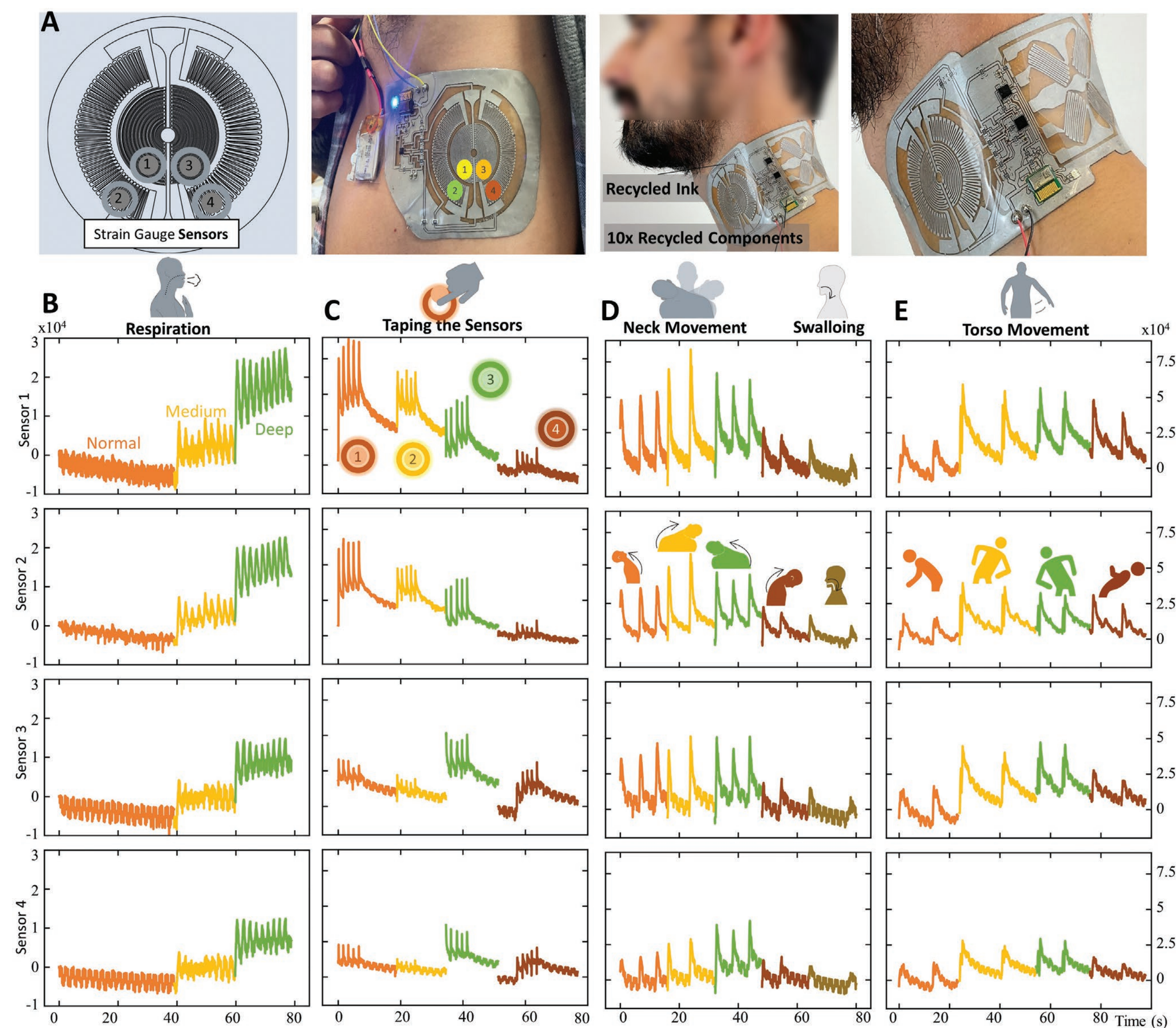

Figure 6. A) Soft-matter chip-integrated multinode sensor patch produced by 1× recycled LM and 10× recycled microchip. Fingerprint of the generated signal during mild, normal, and deep respiration (B), tapping (C), four different neck movements, and swallowing (D), and four different torso movement (E).

Figure 6A and Video S4 (Supporting Information) show examples of two complex 3R circuits that were produced through laser patterning and vapor soldering. Both circuits integrate several laser-patterned strain gauge sensors and all necessary microchips. The circuit in Figure 6A-iii is produced with recycled ink (recovered liquid metal and new silver flakes) and microchips that were integrated into the same circuit and recovered 10 times. Figure 6B shows the digital fingerprint of four strain sensors in 16 different scenarios: mild, medium, and deep respiration (Figure 6B); sequential tapping of the sensors (Figure 6C); neck stretching exercise in four directions and swallowing (Figure 6D); and four types of torso exercise (Figure 6E). Additional details from the sensor and the obtained signals are found in Figures S6–S8 (Supporting Information). A distinct digital fingerprint can be observed in each case, making it even visually classifiable. When combined with advanced machine learning techniques, these patches enable monitoring of vital, behavioral, and psychological signals. At the same time, 3R electronics paves an important step toward sustainable development by enabling a circular economy through the recovery and reuse of the constitutional elements in these patches that are intended to be used only for a short time.

3. Conclusion

This work lays the foundations for the autonomous fabrication of the next generation of 3R electronics. Taking advantage of sinter-free biphasic composites and innovative fabrication techniques based on laser patterning and vapor sintering, we

© 2022 The Authors. Advanced Materials published by Wiley-VCH GmbH

demonstrated the fabrication of condensed soft-matter circuits with integrated microchips that are highly stretchable, resilient, repairable, and recyclable. Compared to digital printing, the laser sintering technique presented in this work offers 10× better resolution and considerably faster patterning. We demonstrated that the laser patterning and soldering techniques could be easily scaled for the rapid fabrication of multiple circuits. Laser patterning of small/medium circuits (most of the circuits shown in this work) takes less than 3 min, and soldering was performed in 30–45 min.

We believe that the presented fabrication techniques are simpler than the existing techniques, not only compared to the existing methods for soft electronics, but also when compared to the rigid PCB manufacturing. Eliminating the need for thermal sintering, thermal soldering, and solder paste deposition contribute to the reduction of multiple fabrication steps. However, the presented techniques are still in their infancy and require further technological development to reach the same maturity as the current high throughput PCB technology. Elimination of the thermal processes from the entire procedure is a critical advancement in the move toward sustainable electronics, as it opens doors for many heat-sensitive elastomers that could not withstand sintering or soldering temperature. This includes emerging recyclable and biodegradable polymers/elastomers.[21,28,29]

These circuits are resilient to mechanical strain and repairable if cut. We demonstrated that traces printed using this material architecture could withstand 1700% of strain, and microchip-integrated circuits can withstand a record-breaking maximum strain value of ≈900%. When cut, these circuits are healed through the vapor exposure technique. The healing is so efficient that the circuits can be subjected to mechanical strain post-healing. When disposed of, these circuits can be processed through simple techniques that allow them to recover their constitutional elements, including textiles, metals, and microchips. We showed an example of a complex patch with multiple laser patterned strain gauges that integrate microchips that have been recycled 10 times. It is noteworthy that the 3R principle is only partially applied to the microchip-integrated circuits, as the microchips themselves are not soft, resilient and repairable, but they can be recycled.

As examples of emerging applications, we demonstrated the fabrication of complex chip-integrated epidermal patches that can obtain a fingerprint of optical, thermal, and mechanical signals from the human skin for human health monitoring and activity classification.

4. Experimental Section

Synthesis of Biphasic Composites: EGaIn–Ag–SIS composite was prepared by dissolving SIS (14 wt% Sigma Aldrich) in toluene (15% SIS) until a clear solution was obtained. For each 5 g of the BCP solution, 6.2 g of Ag flakes (Silflake 071 Technic Inc.) and 15 g of EGaIn were added and mixed using a planetary mixer (2000 rpm).

Similar method to previous composite was followed to prepare EGaIn–Fe–SIS, replacing Ag flakes with magnetite particles (Fe3O4), (52 μm size, 99%, CAS: 1309-38-2).

Direct Digital Printing: 5cc Ink cartridges were filled with the corresponding ink, then printing was performed using a Voltera V-One. The settings used were based upon manufacturer guidelines (adapted to the correspondent composite, based on viscosity). To achieve a highly conductive uniform circuit, usually two to three layers were required. After printing, the circuits were usually cured for 45 min^{-1} h in an oven (60 °C), or overnight at room temperature

Electromechanical Characterization: To characterize the electromechanical performance of the materials, a "Dogbone" shape was used with the Die C ASTM D 412 standard as basis. "dog bones" were made by laser patterning (VLS 3.50, Universal Laser Systems Inc) 1 mm thick films. The films were produced by applying a thin-film applicator to the latex prepolymer (Elastica PVS Latex) with dimensions (1 × 50 mm track with 4.0 × 3.5 mm pads). For electromechanical testing, an Instron 5969 with a 100 N load cell and a data acquisition system composed of a multimeter (gw nstek gdm-8351) and 16-bit DAQ(NI USB 6002) was used.

SEM Microscopy: The surface and cross-section morphologies of the samples were characterized by scanning electron microscopy (SEM) using a FEI Quanta 400FEG ESEM equipped with an EDAX Genesis X4M. For the cross-section observation the samples were immersed for 90 s in liquid nitrogen. This allowed for a clean fracture of the samples to be made through mechanical impact.

Optical Microscopy: Microscopic imaging was used for characterization of the morphology of the deposited composites. It was done using a Leica S9D stereomicroscope, with up to 55× magnification, coupled with a MU900 AmScope 9.0MP camera, and AmScope software for image capture and measuring.

PVA: 5 g of PVA powder (Selvol 125, SEKISU) was mixed with 50 mL of H_2O. The mixture was stirred at 90 °C using a hot plate (AGIMATIC-N) until it became a clear and homogeneous solution.

Conductive Ink: The ink was prepared by dissolving SIS in toluene (20 wt% SIS) until a clear solution was obtained. For each 5 g of BCP solution, 6.2 g of Ag flakes (Silflake, Technic) and 15 g of EGaIn were added and mixed using a planetary mixer (Thinky ARE-250) at 2000 rpm.

SIS Substrate Solution: The SIS solution was prepared using a 1:2 ratio of SIS (Styrene 14%, Sigma Aldrich) and toluene.

Patch Fabrication, Laser Patterning: The fabrication started by first applying a 300 μm PVA solution over the glass, using a thin-film applicator (ZUA 2000, ZEHNTNER). This layer served as the sacrificial layer that permits easy circuit release. Then, two layers of conductive ink were spread over the PVA using the thin film applicator consecutively. After curing the ink in the oven, the circuit was patterned to isolate the circuit traces by laser ablation (pulsed fiber laser with 1064 nm wavelength) while blowing air to it, in order to expel the created debris. Because the laser wavelength only affects metals, the PVA layer under the ablation area remained intact. This turned out to be an effective method to fabricate high-resolution circuits with spacing as low as 70 μm, thus enabling the possibility of using smaller IC packages in the applications. A 700 μm SIS substrate solution was applied over the circuit using a thin film applicator. After curing, an adhesive Kapton tape was placed on top of the cured circuit to support it mechanically, avoiding overstraining the circuit during the next steps. After peeling the circuit from the glass, the PVA layer was dissolved and removed in water. Using transferable glue, the circuit was attached to the glass with the Kapton side facing down.

Microchip Interfacing: The circuit was populated with SMD components using a pick and place machine (eC-placer Eurocircuits) which were then "soldered" in a toluene vapor chamber for 45 min. The vapor was generated using a homemade setup with room-temperature aerosol generator with the desired profile of intensity. At these stage components were soldered into the ink, and mechanical locked, thanks to the adhesive properties of the SIS. After "soldering," the circuit was sealed using substrate solution of SIS. The circuit is left at tilted position in order to remove the excess material by gravity.

Multi Strain Senso: The circuit consisted of a Bluetooth module (CYBLE-014008-00 from Cypress) and two 24 bits ADC (ADS122C04 from Texas Instruments) to measure the analogue signals from the strain sensors. The values from each sensor were captured and sent wirelessly to a PC. The strain sensors were patterned as part of the conductive circuit. The strain sensors consisted in a foil patterned design, as the foil

© 2022 The Authors. Advanced Materials published by Wiley-VCH GmbH

deforms, the electrical resistance changes due to its dependence to the conductor geometry.

SpO2 Patch: The circuit measured oxygen saturation. It used light with two different wavelengths pointed to parts of the body with high blood flow rate and measured the absorbance using photodetectors. The system comprised several light emitters in the red and infrared band, controlled by a specialized SpO2 IC (MAXM86146 from Maxim) containing two high sensitivity photodiodes. A Bluetooth module (CYBLE-022001-00 from Cypress) was integrated to the patch to wirelessly exchange information with the host computer.

Temperature Monitoring Circuit: The circuit measures wireless temperature and humidity with integrated Bluetooth (CYBLE-022001-00 from Cypress), battery, temperature, and humidity sensor (Si7020-A20 from Silicon Labs), which sends the data wirelessly to a mobile phone application.

Recycling e-Patch: The polymer substrate and encapsulation removal were done by placing the circuit on top of a filter (mesh count 100T) and paper towel (soaked with liquid toluene), positioned inside of an enclosed 1 L volume chamber. The chamber setup was left in the oven at 60 °C for 2 h. During this time the polymer turned into a liquid and settled down due to gravity, passing through the filter mesh leaving the SMD components and ink exposed. The filter with the remaining circuit on top was taken from the chamber, the SMD components were collected using a tweezer and ink metals were removed with a spatula.

Recycling e-Textile: The polymer substrate and encapsulation removal were done by placing the circuit on top of a filter (mesh count 100T) and paper towel (soaked with liquid toluene), positioned inside of an enclosed 1 L volume chamber. The chamber setup was left in the oven at 60 °C for 2 h. During this time the polymer turned into a liquid and settles down due to gravity, passing through the filter mesh leaving the SMD components and ink exposed. The filter with the remaining circuit on top was taken from the chamber, the SMD components were collected using a tweezer and ink metals were removed with a spatula.

Recycling e-Textile: The circuit was separated from the textile by first impregnating the textile with acetone in order to dissolve the TPU glue layer and detach it from the textile. The circuit was then removed by hand. The two TPU sheets containing the conductive ink circuit and SMDs was immersed inside of a flask filled with acetone. The flask was manually shake for 2 min and then the sealing and substrate TPU layers were detached from each other by hand. Most of the SMD components were released from the substrate during process, although, to completely separate the ink and SMD components, additional immersion and shaking was done until all SMDs and ink were released from the TPU sheets. Components and ink were recovered from the bottom of the flask using a tweezer.

Recycling EGaIn–Fe–SIS Ink: After removing the metal chunk from the circuit, using the methods explained in Figure 5, the LM-Ferrite-SIS waste was mixed into a Citric acid and isopropanol solution (2000 RPM for 3 min, Thinky Planetary mixer). Most of the LM droplets were extracted. The remaining metal rich chunk was washed with water, and put in Toluene and subjected to mixing at 2000 RPM for 3 min in order to separate the remaining SIS from other components. Finally, the magnetic particles were collected by applying an external magnet, washed with water, and dried in an oven for further use.

Recycling EGaIn–Ag–SIS Ink: After removing the metal chunk from the circuit, using the methods explained in Figure 5, the LM-Ag flake-SIS ink waste was mixed in 1 M NaOH solution at 2000 RPM for 3 min. At this stage, most of LM droplets were extracted. After removing the NaOH, the rest of the waste was put in acetic acid accompanied by Epsom salt, and subjected to mixing at 2000 RPM for 3 min. Additional LM droplets were extracted. This step allowed the resulting slurry to be decomposed. In order to extract additional LM from the waste, the metal chunk in Isopropanol (40 W for 5 min) was sonicated to induce additional mechanical shear forcing to produce LM nano particles, similar to previous works on fabrication of EGaIn Nanoparticles. The mixed solution was dried in an oven and crushed into fine powders, and dispersed in Toluene (2000 RPM for 3 min). At this stage, all the materials almost decomposed, which was followed by adding HCl. HCL allowed removal of the gallium oxide shell of the EGaIn Nano particles, resulting in aggregation into a larger droplet that can be collected. The rest of the material was an Ag rich chunk that is sent to the leaching and electrowinning process.

Acid Leaching: To form a suspension containing dissolved particles from the recovered metal chunk, 1 mL of THF was added into a 20 mL flask along with the metal chunk, and mixed (Thinky ARE-250, 500 rpm, 30 min), to dissolve the remaining of the polymer and separate the metal particles. A sonicator was used to further disperse the particles (20 min 60% power). The mixture was filled with DI water to a total volume of 20 mL prior to sonication. 2 mL of HHO was added drop by drop to the suspension while stirring immersed in a water bath. The mixture was then heated at 70 °C using a hot plate for an additional 20 min while stirring. Then, 2 mL of H_2SO_4 was added drop by drop and stirred for 1 h to completely dissolve the metals.

Electrowinning: The solution was poured on an electrochemical cell container and glassy carbon electrodes were used as electrodes for cathode and anode. Recovery of Ag was achieved by applying a constant potential of 10 V for 4 h. At the cathode surface the deposition of pure Ag metal aggregates and forms a metal chunk which normally falls to the bottom of the container, which was removed using a spatula.

Supporting Information

Supporting Information is available from the Wiley Online Library or from the author.

Acknowledgements

This work was partially supported by the Foundation of Science and Technology (FCT) of Portugal through the CMU-Portugal project WoW (Reference Nr: 45913), and Dermotronics (PTDC/EEIROB/31784/2017), financed by the EU structural & investment Funds (FEEI) through operational program of the center region. Financing also came from the SMART Display project (reference: POCI-01-0247-FEDER-047153), cofinanced by the European Regional Development Fund, through Portugal 2020 (PT2020), and by the Competitiveness and Internationalization Operational Programme (COMPETE 2020). The experiments involving human subject and depicted in Figures 2 and 6 are performed with the full, informed consent of the participant.

Conflict of Interest

The authors declare no conflict of interest.

Data Availability Statement

The data that support the findings of this study are available from the corresponding author upon reasonable request.

Keywords

biphasic liquid metal, electronic waste, recyclable electronics, soft-matter electronics, wearable biomonitoring

Received: April 11, 2022
Revised: May 19, 2022
Published online: June 27, 2022

[1] Y. Hong, D. Thirion, S. Subramanian, M. Yoo, H. Choi, H. Y. Kim, J. F. Stoddart, C. T. Yavuz, *Proc. Natl. Acad. Sci. USA* **2020**, *117*, 16174.
[2] B. Ghosh, M. K. Ghosh, P. Parhi, P. S. Mukherjee, B. K. Mishra, *J. Cleaner Prod.* **2015**, *94*, 5.

© 2022 The Authors. Advanced Materials published by Wiley-VCH GmbH

[3] X. Aeby, A. Poulin, G. Siqueira, M. K. Hausmann, G. Nyström, *Adv. Mater.* **2021**, *33*, 2101328.
[4] Z. Wang, C. Peng, K. Yliniemi, M. Lundström, *ACS Sustainable Chem. Eng.* **2020**, *8*, 15573.
[5] U. U. Jadhav, H. Hocheng, *J. Achiev. Mater. Manuf. Eng.* **2012**, *54*, 159.
[6] A.-G. Ghica, E. Vasile, C. Carata, C. I. Covaliu, M.-i. Petrescu, G. Iacob, M. Buzatu, *Rom. J. Mater.* **2020**, *50*, 354.
[7] S. Y. Cho, W. G. Lee, P. P. Sun, *Mater. Trans.* **2019**, *60*, 1090.
[8] Z. Wang, P. Halli, P. Hannula, F. Liu, B. P. Wilson, K. Yliniemi, M. Lundström, *J. Electrochem. Soc.* **2019**, *166*, E266.
[9] J. Miao, H. Liu, Y. Li, X. Zhang, *ACS Appl. Mater. Interfaces* **2018**, *10*, 23037.
[10] Y. S. Choi, R. T. Yin, A. Pfenniger, J. Koo, R. Avila, K. B. Lee, S. W. Chen, G. Lee, G. Li, Y. Qiao, A. Murillo-Berlioz, A. Kiss, S. Han, S. M. Lee, C. Li, Z. Xie, Y.-Y. Chen, A. Burrell, B. Geist, H. Jeong, J. Kim, H.-J. Yoon, A. Banks, S.-K. Kang, Z. J. Zhang, C. R. Haney, A. V. Sahakian, D. Johnson, T. Efimova, Y. Huang, et al., *Nat. Biotechnol.* **2021**, *39*, 1228.
[11] C. Shi, Z. Zou, Z. Lei, P. Zhu, W. Zhang, J. Xiao, *Sci. Adv.* **2020**, *6*, eabd0202.
[12] L. Teng, S. Ye, S. Handschuh-Wang, X. Zhou, T. Gan, X. Zhou, *Adv. Funct. Mater.* **2019**, *29*, 1808739.
[13] W. B. Han, J. H. Lee, J. W. Shin, S. W. Hwang, *Adv. Mater.* **2020**, *32*, 2002211.
[14] K. Liu, H. Tran, V. R. Feig, Z. Bao, *MRS Bull.* **2020**, *45*, 96.
[15] G. Chen, G. Chen, X. Deng, L. Zhu, S. Handschuh-Wang, T. Gan, B. Wang, Q. Wu, H. Fang, N. Renc, X. Zhou, *J. Mater. Chem. A* **2021**, *9*, 10953.
[16] R. Tutika, A. B. M. T. Haque, M. D Bartlett, *Commun. Mater.* **2021**, *2*, 1.
[17] H. Chang, P. Zhang, R. Guo, Y. Cui, Y. Hou, Z. Sun, W. Rao, *ACS Appl. Mater. Interfaces* **2020**, *12*, 14125.
[18] M. Tavakoli, M. H. Malakooti, H. Paisana, Y. Ohm, D. G. Marques, P. Alhais Lopes, A. P. Piedade, A. T. de Almeida, C. Majidi, *Adv. Mater.* **2018**, *30*, 1801852.
[19] P. A. Lopes, D. F. Fernandes, A. F. Silva, D. G. Marques, A. T. de Almeida, C. Majidi, M. Tavakoli, *ACS Appl. Mater. Interfaces* **2021**, *13*, 14552.
[20] P. A. Lopes, S. Bruno, A. T. de Almeida, C. Majidi, M. Tavakoli, *Nat. Commun.* **2021**, *12*, 1.
[21] S. Chen, Z. Wu, C. Chu, Y. Ni, R. E. Neisiany, Z. You, *Adv. Sci.* **2022**, *9*, 2105146.
[22] M. J. Ford, D. K. Patel, C. Pan, S. Bergbreiter, C. Majidi, *Adv. Mater.* **2020**, *32*, 2002929.
[23] K. B. Ozutemiz, J. Wissman, O. B. Ozdoganlar, C. Majidi, *Adv. Mater. Interfaces* **2018**, *5*, 1701596.
[24] B. Zhang, Q. Dong, C. E. Korman, Z. Li, M. E. Zaghloul, *Sci. Rep.* **2013**, *3*, 1098.
[25] J. Jiang, B. Bao, M. Li, J. Sun, C. Zhang, Y. Li, F. Li, X. Yao, Y. Song, *Adv. Mater.* **2016**, *28*, 1420.
[26] D. G. Marques, P. A. Lopes, A. T. Almeida, M. de Carmel, M. Tavakoli, *Lab Chip* **2019**, *19*, 897.
[27] T. Lu, J. Wissman, C. Majidi, *ACS Appl. Mater. Interfaces* **2015**, *7*, 26923.
[28] J. A. Chiong, H. Tran, Y. Lin, Y. Zheng, Z. Bao, *Adv. Sci.* **2021**, *8*, 2101233.
[29] Y. Deng, R. Dewil, L. Appels, R. Ansart, J. Baeyens, Q. Kang, *J. Environ. Manage.* **2021**, *278*, 111527.

© 2022 The Authors. Advanced Materials published by Wiley-VCH GmbH